

# ControlFusion: A Controllable Image Fusion Framework with Language-Vision Degradation Prompts

Lin Feng Tang<sup>1\*</sup> Yeda Wang<sup>1\*</sup> Zhanchuan Cai<sup>2</sup> Junjun Jiang<sup>3</sup> Jiayi Ma<sup>1†</sup>

<sup>1</sup>Wuhan University <sup>2</sup>Macau University of Science and Technology <sup>3</sup>Harbin Institute of Technology  
 linfeng0419@gmail.com wangyeda@whu.edu.cn zccai@must.edu.mo  
 jiangjunjun@hit.edu.cn jyama2010@gmail.com

## Abstract

Current image fusion methods struggle to address the composite degradations encountered in real-world imaging scenarios and lack the flexibility to accommodate user-specific requirements. In response to these challenges, we propose a controllable image fusion framework with language-vision prompts, termed ControlFusion, which adaptively neutralizes composite degradations. On the one hand, we develop a degraded imaging model that integrates physical imaging mechanisms, including the Retinex theory and atmospheric scattering principle, to simulate composite degradations, thereby providing potential for addressing real-world complex degradations from the data level. On the other hand, we devise a prompt-modulated restoration and fusion network that dynamically enhances features with degradation prompts, enabling our method to accommodate composite degradation of varying levels. Specifically, considering individual variations in quality perception of users, we incorporate a text encoder to embed user-specified degradation types and severity levels as degradation prompts. We also design a spatial-frequency collaborative visual adapter that autonomously perceives degradations in source images, thus eliminating the complete dependence on user instructions. Extensive experiments demonstrate that ControlFusion outperforms SOTA fusion methods in fusion quality and degradation handling, particularly in countering real-world and compound degradations with various levels.

## 1. Introduction

Image fusion is a crucial technique in image processing. By effectively leveraging complementary information from multiple sources, the limitations associated with information collection by single-modal sensors can be significantly mitigated [40]. Among the various research areas within

\*Equal contribution.

†Corresponding author.

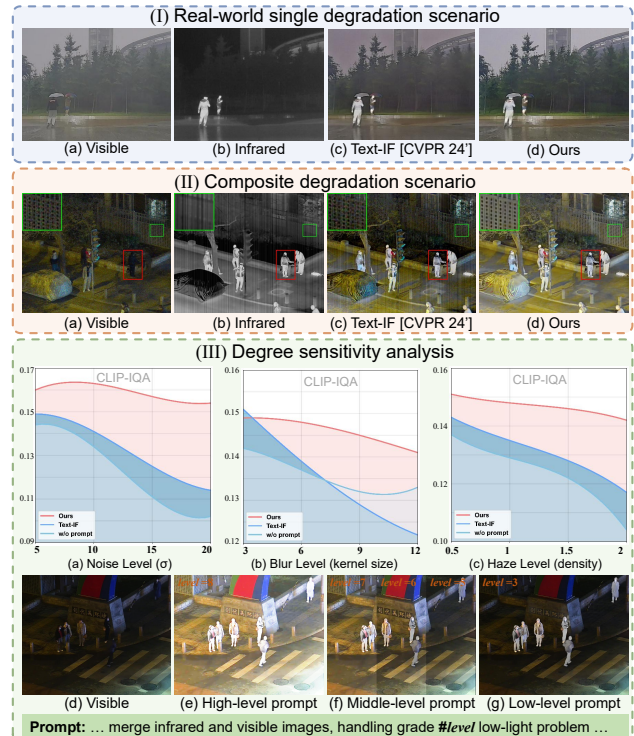


Figure 1. Fusion performance comparison across real-world, composite degradation, and varying degradation levels.

this field, infrared-visible image fusion (IVIF) has garnered considerable attention. IVIF integrates essential thermal information from infrared (IR) images with the intricate texture details from visible (VI) images, offering a richer and more complete depiction of the scene [44]. By harmonizing diverse information and producing visually striking results, IVIF has found extensive applications in areas such as security surveillance [45], military detection [23], scene understanding [7, 43], and assisted driving [1], *etc.*

Recently, IVIF has emerged as a focal point of research, leading to rapid advancements in related methods. Based on the architecture of deep networks, these methods

can be categorized into convolutional neural network- [14, 50], autoencoder- [11, 12], generative adversarial network- [15, 19], Transformer- [21, 42], and diffusion model-based [41, 49] methods. Besides, from a functional perspective, they can be categorized into visual-oriented [30, 50], joint registration-fusion [28, 37], semantic-driven [16, 29], and degradation-robust [32, 41] schemes.

Notably, although degradation-robust schemes can mitigate degradation interference to some extent, they still have certain limitations. On the one hand, these methods often rely on simplistic approaches to construct training data, overlooking the domain gap between simulated data and realistic images, which significantly hampers their generalizability in practical scenarios, as presented in Fig. 1(I). On the other hand, they are tailored for specific or single types of degradation, making them ineffective in handling more complex composite degradations, as illustrated in Fig. 1(II). Last but not least, as shown in Fig. 1(III), existing methods lack degradation level modeling, causing a sharp decline in performance as degradation intensifies. Furthermore, these approaches do not offer the flexibility to dynamically adjust fusion results according to the diverse perceptual requirements of different users.

To overcome these limitations, we propose a versatile and controllable fusion model based on language-vision prompts, termed ControlFusion. On the one hand, we introduce a physics-driven degraded imaging model, which accurately simulates the physical mechanisms of the actual degradation process, *e.g.*, illumination-, weather-, and sensor-related distortions. The proposed model not only effectively bridges the gap between synthetic data and real-world images but also offers valuable data support for handling complex composite degradations. On the other hand, we develop a prompt-modulated image restoration and fusion network to generate high-quality fusion results. The prompt-modulated module enables our network to dynamically adjust feature distribution based on degradation characteristics (which can be specified by users), achieving robust feature enhancement. This also allows our method to respond to diverse user requirements. Furthermore, we devise a spatial-frequency visual adapter that combines frequency-domain degradation priors to directly extract degradation cues from degraded inputs, eliminating the heavy reliance on user instructions, as customizing prompts for each scene is time-consuming and labor-intensive. As shown in Fig. 1, benefiting from the aforementioned designs, our method excels in handling both real-world and composite degradation scenarios, and it shows strong robustness across various degradation levels. In summary, our main contributions are as follows:

- We propose ControlFusion, a versatile image restoration and fusion framework that uniformly models diverse degradation types and degrees, using textual and visual

prompts as a medium. Specifically, its controllability enables it to respond to user-specific customization needs.

- A spatial-frequency visual adapter is devised to integrate frequency characteristics and directly extract text-aligned degradation prompts from visual images, enabling large-scale automated deployment.
- A physics-driven imaging model is developed, integrating physical mechanisms such as the Retinex theory and atmospheric scattering principle to bridge the gap between synthetic data and real-world images, while providing data support for addressing composite degradations.

## 2. Related Work

**Image Fusion.** Earlier visual-oriented fusion approaches primarily concentrated on merging complementary information from multiple modalities and improving visual fidelity. These methods often depend on sophisticated network architectures and carefully designed loss functions to ensure that the integrated content retains the essential characteristics of the original images, preserving their unique features while enhancing overall quality. The mainstream network architectures primarily include CNN-based [20, 47], AE-based [12, 48], GAN-based [15, 19], Transformers [21] and diffusion models [49]. Furthermore, several schemes including joint registration and fusion [33, 37], semantic-driven [15, 29], and degradation-robust [32, 38, 41] methods, are proposed to broaden the practical applications of image fusion. For instance, Tang et al. [31] and Liu et al. [17] developed corresponding solutions for illumination distortions and noise interference, respectively. In addition, Yi et al. [38] proposed a unified image restoration and fusion network to address various degradations. However, they are unable to handle mixed degradations and struggle to generalize to real-world scenarios. In particular, Text-IF [38] relies on tedious manual efforts to customize text prompts for each scene, hindering large-scale automated deployment.

**Image Restoration with Vision-Language Models.** With the advancement of deep learning toward multimodal integration, the image restoration field has progressively evolved into a new paradigm of text-driven schemes. CLIP [26] establishes visual-textual semantic representation alignment through dual-stream Transformer encoders pre-trained on 400 million image-text pairs. This framework lays the foundation for the widespread adoption of *Prompt Engineering* in computer vision. Recent studies integrate CLIP encoders with textual user instructions, proposing generalized restoration frameworks including PromptIR [24], AutoDIR [9], and InstructIR [2], which effectively handle diverse degradation types. Moreover, SPIRE [25] further introduces fine-grained textual restoration cues by quantifying degradation severity levels and supplementing semantic information for precision restora-

tion. To eliminate reliance on manual guidance, Luo et al. [18] developed DA-CLIP by fine-tuning CLIP on mixed-degradation datasets, enabling degradation-aware embeddings to facilitate distortion handling. However, existing unified restoration methods are primarily designed for natural images, which exhibit notable limitations when processing multimodal image pairs (e.g., infrared-visible).

### 3. Physics-driven Degraded Imaging Model

#### 3.1. Imaging Formulation

In real-world scenarios, images are often affected by multiple degradation factors simultaneously, which leads to sub-optimal performance of restoration and fusion methods designed for isolated degradations. To tackle the complex and variable degradation challenges, we propose a physics-driven imaging model aimed at reducing the domain gap between simulated data and real-world imagery. Visible (VI) images are typically degraded by illumination conditions (low-light, overexposure), weather (rain, haze), and sensor-related issues (noise, blur), while infrared (IR) images usually suffer from sensor-related interference, such as stripe noise and low contrast. Thereby, given a clear image  $I_m (m \in \{ir, vi\})$ , the proposed imaging model can be mathematically represented as:

$$D_m = \mathcal{P}_s (\mathcal{P}_w (\mathcal{P}_i (I_m))), \quad (1)$$

where  $D_m$  is the corresponding degraded image, and  $\mathcal{P}_i$ ,  $\mathcal{P}_w$ , and  $\mathcal{P}_s$  represent illumination-, weather-, and sensor-related distortions, respectively.

**Illumination-related Distortions.** Following the theoretical framework of Retinex, the formation of illumination-degraded images  $D_{vi}^i$  is mathematically modeled as:

$$D_{vi}^i = \mathcal{P}_i(I_{vi}) = \frac{I_{vi}}{L} \cdot L^\gamma, \quad (2)$$

where  $L$  is the illumination map estimated by LIME [5].  $\gamma \in [0.5, 3]$  controls the illumination level.

**Weather-related Distortions.** According to the methodologies in [13, 22], we employ the following formula to simulate weather-related degradations (i.e. rain and haze):

$$D_{vi}^w = \mathcal{P}_w(I_{vi}) = I_{vi} \cdot t + A(1 - t) + R, \quad (3)$$

where  $t$  and  $A$  denote the transmission map and atmospheric light, respectively. And  $t$  is defined by the exponential decay of light, expressed as  $t = e^{-\beta d(x)}$ , where the haze density coefficient  $\beta \in [0.5, 2.0]$ .  $d(x)$  refers to the scene depth, estimated by DepthAnything-V2 [39]. Besides,  $A$  is constrained within  $[0.3, 0.9]$  for realistic simulation.

**Sensor-related Distortions.** Sensor-related distortions encompass various types of noise, motion blur, and contrast degradation. Contrast degradation and stripe noise of infrared images can be modeled as:

$$D_{ir}^s = \mathcal{P}_s(I_{ir}) = \alpha \cdot I_{ir} + \mathbf{1}_H \mathbf{n}^\top, \quad (4)$$

where  $\alpha$  is a constant less than 1 for contrast reduction,  $\mathbf{1}_H \in \mathbb{R}^H$  is an all-ones column vector and  $\mathbf{n} \in \mathbb{R}^W$  represents the column-wise Gaussian noise vector sampled from  $\mathcal{N}(0, \epsilon^2)$  with  $\epsilon \in [1, 15]$ . Moreover, Gaussian noise and motion blur in source images can be modeled as:

$$D_m^s = \mathcal{P}_s(I_m) = I_m * K(N, \theta) + \mathcal{N}(0, \sigma^2), \quad (5)$$

where  $\mathcal{N}(0, \sigma^2)$  represents Gaussian noise with  $\sigma \in [5, 20]$ .  $*$  denotes convolution with a blur kernel  $K(N, \theta) = \frac{1}{N} R_\theta(\delta_c \otimes \mathbf{1}_N)$  constructed by rotating an impulse  $\delta_c \otimes \mathbf{1}_N$  with random angle  $R_\theta$  ( $\theta \in [10, 80]$ ), using  $\frac{1}{N}$  to normalize the kernel energy. Here,  $N \in [3, 12]$  controls the blur level.

#### 3.2. Composite Degradation Dataset with Levels

Based on Eq. (1), we construct a multi-modal composite Degradation Dataset with four Levels (DDL-12), comprising 12 distinct degradations along with their corresponding high-quality images. In particular, we select 2,050 high-quality clear images from multiple publicly available infrared-visible datasets [8, 16, 30, 36]. Subsequently, the degraded imaging model is employed to synthesize degraded images with 12 types and 4 levels of degradation. Finally, the DDL-12 dataset contains approximately 32,000 training image pairs and 4,000 test image pairs.

## 4. Methodology

### 4.1. Problem Formulation

Given two source images  $I_{ir} \in \mathbb{R}^{H \times W \times 1}$  and  $I_{vi} \in \mathbb{R}^{H \times W \times 3}$ , the typical fusion paradigm employs a deep network  $\mathcal{N}_f$  to integrate complementary information and synthesize the fused image  $I_f$ , expressed as:

$$I_f = \mathcal{N}_f(I_{ir}, I_{vi}). \quad (6)$$

However, in complex scenarios, source images usually suffer from degradation interference, thus the advanced fusion paradigm must take both image restoration and information aggregation into account. Concatenation and coupling are two common approaches to implement this. Notably, while the concatenation approach is straightforward, it neglects the intrinsic relationship between restoration and fusion, frequently yielding suboptimal outcomes. As illustrated in Fig. 2, we propose a controllable paradigm that couples restoration and fusion with degradation prompt, termed ControlFusion, to overcome this limitation. On the one hand, the coupled approach enhances task synergy. On the other hand, leveraging degradation prompts to modulate the restoration and fusion process enables the network to adapt to diverse degradation distributions while meeting user-specific customization requirements. Thus, the proposed restoration and fusion paradigm can be defined as:

$$I_f = \mathcal{N}_{rf}(I_{ir}, I_{vi}, p | \Omega), \quad (7)$$

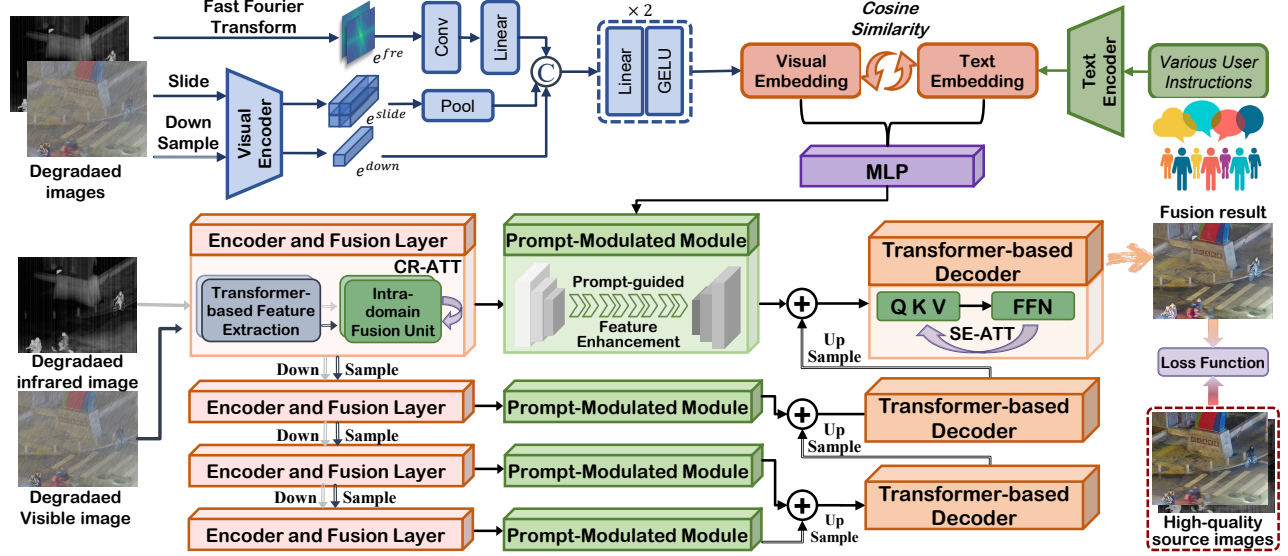


Figure 2. The overall framework of our semantic and degradation dual-prior guided image fusion network.

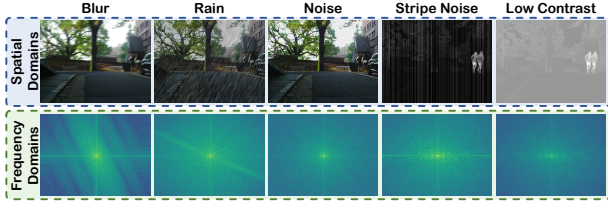


Figure 3. The visualization of various types of degradation in the spatial and frequency domains.

where  $\mathcal{N}_{r,f}$  is a restoration and fusion network,  $P$  denotes degradation prompts, and  $\Omega$  indicates the degradation set. Notably, degradation prompts can be either user-specified text or directly extracted from input images, greatly enhancing the flexibility of our framework without heavily relying on user instructions. To fully harness its potential, our ControlFusion employs a two-stage optimization protocol. Stage I aligns textual prompts with visual embedding, while Stage II optimizes the overall framework.

#### 4.2. Stage I: Textual-Visual Prompts Alignment

**Text Semantic Encoder.** Adopting text to represent the degradation type and degree is the most straightforward approach. Thus, we introduce a pre-trained vision-language model (*i.e.*, CLIP [26]), to achieve prompt embedding. Given a user instruction  $T_{instr}$ , the text semantic encoder  $\mathcal{E}_t$  from CLIP is deployed to convert it into a text embedding:

$$p_{text} = \mathcal{E}_t(T_{instr}). \quad (8)$$

**Spatial-Frequency Collaborative Visual Adapter.** It is important to emphasize that customizing text instructions for each image is extremely time-consuming and labor-intensive. Therefore, we expect to develop a textual-visual

adapter that directly extracts visual embeddings from source images that align with  $p_{text}$ , enabling automated deployment. In particular, as shown in Fig. 2, images with different degradations in the same scene exhibit distinct spectral characteristics, indicating that frequency features contain rich degradation priors. To this end, we devise a spatial-frequency collaborative visual adapter (SFVA) to extract visual prompts. In the frequency branch, we utilize the Fast Fourier Transform (FFT) algorithm in conjunction with a CNN to extract frequency features  $F_{fre}$ :

$$\begin{aligned} F_{fre}^m &= \sum_{x=0}^{W-1} \sum_{y=0}^{H-1} D_m(x, y) e^{-j2\pi(\frac{ux}{W} + \frac{vy}{H})}, \\ F_{fre} &= \text{Linear}(\text{Conv}([F_{fre}^{ir}, F_{fre}^{vi}])), \end{aligned} \quad (9)$$

where  $[\cdot, \cdot]$  denotes channel-wise concatenation. In the spatial branch, we employ cropping and downsampling for data augmentation, followed by a CNN-based visual encoder to extract spatial features  $F_{spa}$ . Then, we concatenate  $F_{fre}$  and  $F_{spa}$ , and apply successive linear layers to obtain the final visual embedding  $p_{vis}$ . Furthermore, we employ MSE loss  $\mathcal{L}_{mse}$  and cosine similarity loss  $\mathcal{L}_{cos}$  to impose constraints on the similarity between  $p_{vis}$  and the pre-defined  $p_{text}$ . The loss for Stage I is formulated as:

$$\mathcal{L}_I = \lambda_1 \underbrace{\|p_{vis} - p_{text}\|^2}_{\mathcal{L}_{mse}} + \lambda_2 \underbrace{\left(1 - \frac{p_{vis} \cdot p_{text}}{\|p_{vis}\| \|p_{text}\|}\right)}_{\mathcal{L}_{cos}}, \quad (10)$$

where  $\lambda_1$  and  $\lambda_2$  are parameters, balancing various losses.

### 4.3. Stage II: Prompt-modulated Restoration and Fusion

#### 4.3.1. Network Architectures

**Feature Encoding and Fusion Layer.** As shown Fig. 2, we devise the hierarchical transformer-based encoders to extract multi-scale feature representations from degraded infrared ( $D_{ir}$ ) and visible ( $D_{vi}$ ) images separately, which is formulated as:

$$\{F_{ir}, F_{vi}\} = \{\mathcal{E}_{ir}(D_{ir}), \mathcal{E}_{vi}(D_{vi})\}, \quad (11)$$

where  $\mathcal{E}_{ir}$  and  $\mathcal{E}_{vi}$  are infrared and visible image encoders.

Furthermore, to achieve comprehensive cross-modal feature integration, we design the intra-domain fusion unit, where the cross-attention (CR-ATT) mechanism is employed to facilitate interaction between features across modalities. Specifically, the linear transformation functions  $\mathcal{F}_{ir}^{qkv}$  and  $\mathcal{F}_{vi}^{qkv}$  project  $F_{ir}$  and  $F_{vi}$  into their corresponding  $Q$ ,  $K$ , and  $V$ , expressed as:

$$\begin{aligned} \{Q_{ir}, K_{ir}, V_{ir}\} &= \mathcal{F}_{ir}^{qkv}(F_{ir}), \\ \{Q_{vi}, K_{vi}, V_{vi}\} &= \mathcal{F}_{vi}^{qkv}(F_{vi}). \end{aligned} \quad (12)$$

Subsequently, we swap the queries  $Q$  of complementary modalities to promote spatial interaction:

$$F_f^{ir} = \text{softmax}\left(\frac{Q_{vi}K_{ir}}{\sqrt{d_k}}\right)V_{ir}, F_f^{vi} = \text{softmax}\left(\frac{Q_{ir}K_{vi}}{\sqrt{d_k}}\right)V_{vi}, \quad (13)$$

where  $d_k$  is a learnable scaling factor. Finally, we concatenate  $F_f^{ir}$  and  $F_f^{vi}$  to get fusion features:  $F_f = [F_f^{ir}, F_f^{vi}]$ .

**Prompt-modulated Module.** To dynamically adapt fusion feature distributions to varying degradation patterns and degrees, we propose a prompt-modulated module (PMM) for robust feature enhancement. First, sequential MLPs ( $\Phi_p$ ) are utilized to derive distributional optimization parameters:

$$[\gamma_p, \beta_p] = \Phi_p(p), \quad \text{where } p \in \{p_{vis}, p_{text}\}.$$

Then,  $\gamma_p$  and  $\beta_p$  are applied for feature scaling and bias shifting in a residual manner:

$$\hat{F}_f = (1 + \gamma_p) \odot F_f + \beta_p, \quad (14)$$

where  $\odot$  denotes the Hadamard product, and  $\hat{F}_f$  indicates the enhanced features incorporating degradation prompts.

**Image Decoder.** We further deploy a series of Transformer-based decoder  $\mathcal{D}_f$  with the self-attention mechanism to progressively reconstruct the fused image  $I_f$ :

$$I_f = \mathcal{D}(\hat{F}_f). \quad (15)$$

In particular, PMM and  $\mathcal{D}_f$  are tightly coupled in a multi-stage process, effectively incorporating fusion features and degradation prompts to synthesize the desired image.

#### 4.3.2. Loss Functions

Following the typical fusion paradigm [21, 38], we introduce the intensity loss, structural similarity (SSIM) loss [46], maximum gradient loss, and color consistency loss to constrain the training of Stage II.

The intensity loss  $\mathcal{L}_{int}$  aims to maximize the intensity of fusion results to ensure target prominence, defined as:

$$\mathcal{L}_{int} = \frac{1}{HW} \|I_f - \max(I_{ir}^{hq}, I_{vi}^{hq})\|_1, \quad (16)$$

where  $I_{ir}^{hq}$  and  $I_{vi}^{hq}$  are the high-quality source images in our DDL-12 dataset. The structural similarity loss  $\mathcal{L}_{ssim}$  ensures the fused image maintains structural consistency with the high-quality source images, preserving essential structural information, and is formulated as:

$$\mathcal{L}_{ssim} = 2 - (\text{SSIM}(I_f, I_{ir}^{hq}) + \text{SSIM}(I_f, I_{vi}^{hq})). \quad (17)$$

The maximum gradient loss  $\mathcal{L}_{grad}$  maximizes the retention of key edge information from both source images, generating fusion results with clearer textures, formulated as:

$$\mathcal{L}_{grad} = \frac{1}{HW} \|\nabla I_f - \max(\nabla I_{ir}^{hq}, \nabla I_{vi}^{hq})\|_1, \quad (18)$$

where  $\nabla$  denotes the Sobel operator. Moreover, the color consistency loss  $\mathcal{L}_{color}$  ensures that the fusion results maintain color consistency with the visible image. We convert the image to YCbCr space and minimize the distance between the Cb and Cr channels, expressed as:

$$\mathcal{L}_{color} = \frac{1}{HW} \|\mathcal{F}_{CbCr}(I_f) - \mathcal{F}_{CbCr}(I_{vi}^{hq})\|_1, \quad (19)$$

where  $\mathcal{F}_{CbCr}$  denotes the transfer function of RGB to CbCr.

Finally, the total loss  $\mathcal{L}_{II}$  for Stage II is the weighted sum of the aforementioned losses:

$$\begin{aligned} \mathcal{L}_{II} &= \alpha_{int}(p) \cdot \mathcal{L}_{int} + \alpha_{ssim}(p) \cdot \mathcal{L}_{ssim}(t) \\ &\quad + \alpha_{grad}(p) \cdot \mathcal{L}_{grad} + \alpha_{color}(p) \cdot \mathcal{L}_{color}, \end{aligned} \quad (20)$$

where  $\alpha_{int}(p)$ ,  $\alpha_{ssim}(p)$ ,  $\alpha_{grad}(p)$ , and  $\alpha_{color}(p)$  are semantically regulated hyper-parameters related to the degradation prompt  $p$ . In particular, we dynamically adjust the weights based on degradation characteristics (type and severity), allowing our framework to adaptively focus on both fine-grained details and holistic semantic coherence, thereby effectively addressing diverse degradations.

## 5. Experiments

### 5.1. Experimental Details

**Implementation Details.** Our image restoration and fusion network adopts a four-tier encoder-decoder architecture with channel dimensions progressively increasing from 48 to 384, specifically configured as [48, 96, 192, 384]. During training,  $224 \times 224$  pixel patches are randomly

Table 1. Quantitative comparison results on typical fusion datasets. The best and second-best results are highlighted in Red and Purple.

Methods	MSRS				LLVIP				RoadScene				FMB			
	EN	SD	VIF	Qabf	EN	SD	VIF	Qabf	EN	SD	VIF	Qabf	EN	SD	VIF	Qabf
DDFM [49]	6.431	47.815	0.844	0.643	6.914	48.556	0.693	0.517	6.994	47.094	0.775	0.595	6.426	40.597	0.495	0.442
DRMF [32]	6.268	45.117	0.669	0.550	6.901	50.736	0.786	0.626	6.231	44.221	0.728	0.527	6.842	41.816	0.578	0.372
EMMA [50]	6.747	52.753	0.886	0.605	6.366	47.065	0.743	0.547	6.959	46.749	0.698	0.664	6.788	38.174	0.542	0.436
LRRNet [12]	6.761	49.574	0.713	0.667	6.191	48.336	0.864	0.575	7.185	46.400	0.756	0.658	6.432	48.154	0.501	0.368
SegMiF [16]	7.006	57.073	0.764	0.586	7.260	45.892	0.539	0.459	6.736	48.975	0.629	0.584	6.363	47.398	0.539	0.482
Text-IF [38]	6.619	55.881	0.753	0.656	6.364	49.868	0.859	0.566	6.836	47.596	0.634	0.609	7.397	47.726	0.568	0.528
Text-Difuse [41]	6.990	56.698	0.850	0.603	7.546	55.725	0.883	0.659	6.826	50.230	0.683	0.662	6.888	49.558	0.793	0.653
ControlFusion	7.340	60.360	0.927	0.718	7.354	56.631	0.968	0.738	7.421	51.759	0.817	0.711	7.036	50.905	0.872	0.730

Table 2. Quantitative comparison results in different degraded scenarios with pre-enhancement.

Methods	VI (Blur)				VI (Rain)				VI (Low-light, LL)				VI (Over-exposure, OE)			
	CLIP-IQA	MUSIQ	TReS	SD	CLIP-IQA	MUSIQ	TReS	SD	CLIP-IQA	MUSIQ	TReS	SD	CLIP-IQA	MUSIQ	TReS	SD
DDFM [49]	0.141	39.421	39.047	35.411	0.191	38.836	46.285	36.376	0.156	39.495	41.782	31.759	0.143	43.167	43.440	32.099
DRMF [32]	0.128	40.739	40.968	40.722	0.174	48.164	48.565	41.174	0.143	41.428	37.947	38.287	0.190	48.334	42.582	44.256
EMMA [50]	0.131	43.472	41.744	42.553	0.138	45.824	44.916	43.378	0.158	39.674	44.827	40.857	0.180	46.731	47.616	40.242
LRRNet [12]	0.163	42.981	37.268	45.389	0.185	43.291	41.891	46.285	0.164	40.486	34.836	41.639	0.160	42.548	48.414	42.190
SegMiF [16]	0.152	43.005	43.516	44.000	0.195	40.528	49.094	44.274	0.177	44.073	48.376	44.829	0.166	49.132	38.019	38.484
Text-IF [38]	0.164	44.801	46.542	48.401	0.164	41.287	47.380	49.298	0.163	41.096	49.174	47.257	0.172	40.298	45.599	47.330
Text-Difuse [41]	0.172	44.958	47.699	46.376	0.173	39.243	50.017	47.297	0.192	46.734	50.126	49.883	0.183	39.095	49.596	50.279
ControlFusion	0.184	47.849	50.240	50.287	0.196	52.319	52.465	50.901	0.183	48.420	51.072	53.787	0.191	50.301	52.961	54.218

Methods	VI (Rain and Haze, RH)				IR (Low-contrast, LC)				IR (Random noise, RN)				IR (Stripe noise, SN)			
	CLIP-IQA	MUSIQ	TReS	EN	CLIP-IQA	MUSIQ	TReS	SD	CLIP-IQA	MUSIQ	TReS	EN	CLIP-IQA	MUSIQ	TReS	EN
DDFM [49]	0.158	43.119	44.095	6.897	0.172	44.490	44.545	37.452	0.186	34.059	32.807	6.029	0.209	48.479	32.377	6.399
DRMF [32]	0.171	45.524	43.693	6.230	0.208	43.982	45.561	40.315	0.192	44.617	44.085	5.744	0.187	44.714	43.650	6.354
EMMA [50]	0.169	39.092	46.046	6.517	0.154	48.724	43.113	53.861	0.172	39.666	44.466	6.184	0.153	42.802	44.239	6.382
LRRNet [12]	0.170	48.571	48.973	7.363	0.151	48.718	45.266	51.605	0.158	48.274	37.090	7.295	0.137	46.511	36.610	7.702
SegMiF [16]	0.147	46.139	45.019	7.281	0.160	44.659	51.427	44.448	0.180	42.664	39.496	6.669	0.169	49.887	39.247	6.855
Text-IF [38]	0.178	50.568	50.271	6.956	0.187	49.299	49.266	47.032	0.169	46.647	48.491	6.256	0.161	49.019	47.755	6.085
Text-Difuse [41]	0.175	52.788	53.073	7.470	0.165	50.092	51.715	39.429	0.203	49.278	49.479	6.982	0.194	51.762	49.288	7.089
ControlFusion	0.189	54.287	54.465	7.891	0.196	51.986	52.846	57.827	0.189	50.711	51.668	7.724	0.200	50.097	50.264	7.619

Methods	VI (OE) and IR (LC)				VI (Low-light and Noise, LN)				VI (RH) and IR (RN)				VI (LL) and IR (SN)			
	CLIP-IQA	MUSIQ	TReS	SD	CLIP-IQA	MUSIQ	TReS	EN	CLIP-IQA	MUSIQ	TReS	SD	CLIP-IQA	MUSIQ	TReS	EN
DDFM [49]	0.168	43.814	41.894	36.095	0.172	48.293	31.791	6.298	0.151	33.440	32.134	37.342	0.189	36.433	42.630	5.776
DRMF [32]	0.184	42.399	39.374	40.847	0.201	44.363	43.063	5.875	0.174	43.663	43.858	37.997	0.142	38.241	41.049	5.280
EMMA [50]	0.130	39.892	42.076	43.362	0.174	42.201	43.382	5.838	0.165	39.146	44.458	51.205	0.130	37.367	43.888	6.318
LRRNet [12]	0.136	47.209	42.636	46.684	0.144	46.386	35.779	7.306	0.128	47.954	36.831	49.917	0.154	38.426	35.970	7.007
SegMiF [16]	0.114	44.021	42.256	33.647	0.136	49.178	38.570	5.819	0.147	42.354	39.156	31.717	0.151	41.287	37.079	6.767
Text-IF [38]	0.174	48.808	47.998	48.848	0.217	48.100	47.510	5.204	0.158	45.821	47.626	46.543	0.140	41.429	46.220	5.525
Text-Difuse [41]	0.131	49.021	50.980	47.640	0.185	50.775	48.610	6.440	0.181	48.645	48.937	38.808	0.161	47.734	48.448	6.738
ControlFusion	0.187	50.479	50.298	50.955	0.225	49.333	49.513	7.111	0.179	50.107	51.091	55.417	0.167	50.632	48.971	7.055

cropped as inputs, using a batch size of 12 for 100 epochs. Optimization is performed using the AdamW with an initial learning rate of  $1 \times 10^{-3}$  and gradually reduced to  $1 \times 10^{-5}$  following a cosine annealing schedule. For the loss configuration,  $\lambda_1$  and  $\lambda_2$  are set at a 1 : 3 ratio during Stage I. Additionally,  $\alpha_{int}(p)$ ,  $\alpha_{ssim}(p)$ ,  $\alpha_{grad}(p)$ , and  $\alpha_{color}(p)$  are dynamically adjusted based on degradation prompts.

**Experiment Configurations.** We first evaluate the fusion performance of ControlFusion on four widely used datasets, *i.e.*, MSRS [30], LLVIP [8], RoadScene [35], and FMB [16]. The test set sizes for MSRS, LLVIP, RoadScene, and FMB are 361, 50, 50, and 50, respectively. Four metrics, *i.e.*, EN, SD, VIF, and  $Q_{abf}$ , are used to quantify fusion performance. We compare our method with seven SOTA fusion methods, *i.e.*, DDFM [49], DRMF [32], EMMA [50], LRRNet [12], SegMiF [16], Text-IF [38], and Text-Difuse

[41]. Furthermore, we verify the performance of ControlFusion across various degradations, including blur, rain, over-exposure, and low-light in visible images (VI), as well as low-contrast, random noise, and stripe noise in infrared images (IR). Additionally, we evaluate its effectiveness in handling composite degradation scenarios, such as rain and haze in VI, low light and noise in VI, overexposure in VI, low contrast in IR, low light in VI and stripe noise in IR, as well as rain and haze in VI combined with noise in IR. Each degradation scenario includes 100 test image pairs. We use CLIP-IQA [34], MUSIQ [10], TReS [3], EN, and SD to quantify both restoration and fusion performance. For a fair comparison, we exclusively use the visual prompts to characterize degradation types and severity in the quantitative comparison. Meanwhile, we employ several SOTA image restoration algorithms as preprocessing steps to ad-

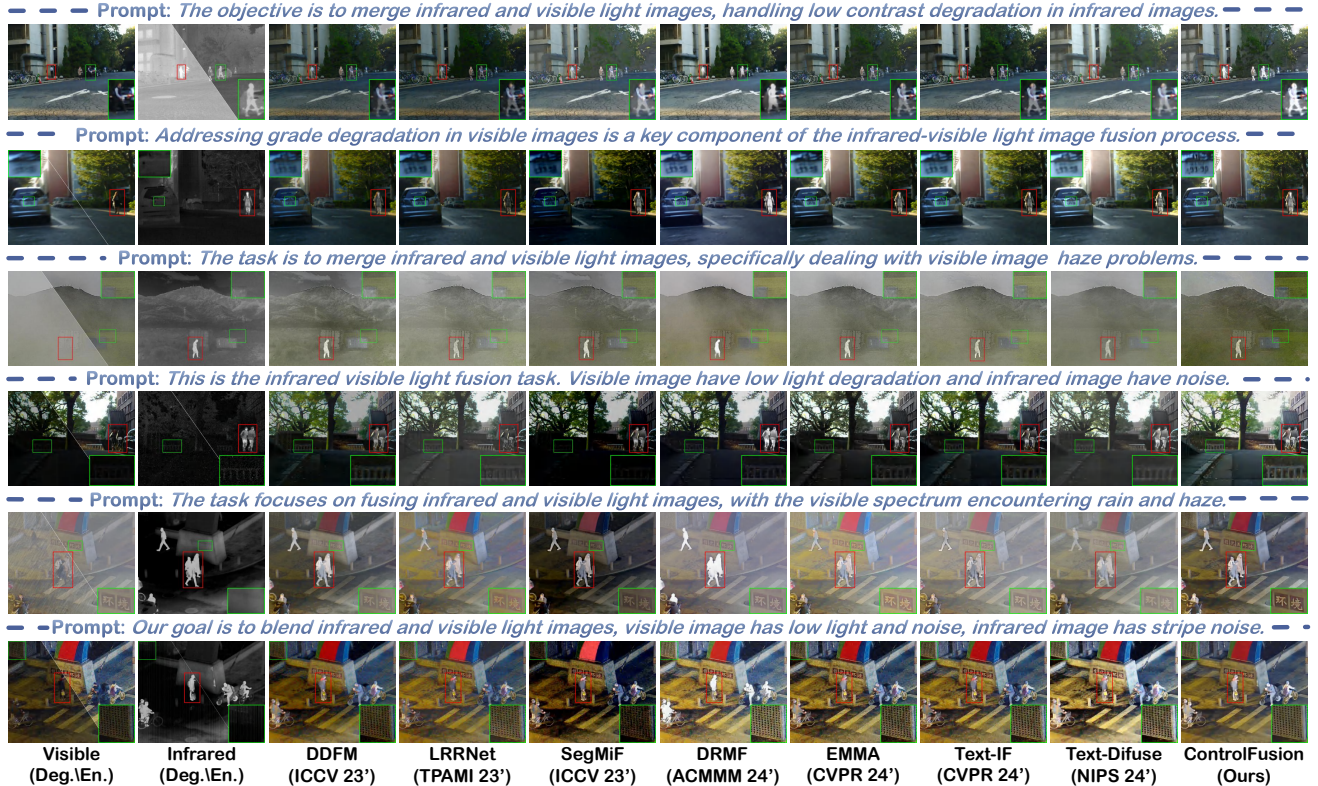


Figure 4. Visualization of fusion results in different degraded scenarios with pre-enhancement.

dress specific degradations. Specifically, OneRestore [6] is used for weather-related degradations, Instruct-IR [2] for illumination-related degradations, and DA-CLIP [18] and WDN [4] for sensor-related degradations. For composite degradations, we select the best-performing method from these algorithms. All experiments are conducted on NVIDIA RTX 4090 GPUs with an Intel(R) Xeon(R) Platinum 8180 CPU (2.50 GHz) using the PyTorch framework.

## 5.2. Fusion Performance Comparison

**Comparison without Pre-enhancement.** Tab. 1 summarizes the quantitative assessment across benchmark datasets. Notably, our method attains SOTA performance in SD, VIF, and  $Q_{abf}$  metrics, showcasing its exceptional ability to maintain structural integrity and edge details. The EN metric remains competitive, indicating that our fusion results encapsulate abundant information.

**Comparison with Pre-enhancement.** The quantitative results in Tab. 2 show that ControlFusion achieves superior CLIP-IQA, MUSIQ, and TReS scores across most degradation scenarios, demonstrating a strong capability in degradation mitigation and complementary context aggregation. Additionally, no-reference fusion metrics (SD, EN) show that ControlFusion performs on par with SOTA methods. Qualitative comparisons in Fig. 4 indicate that ControlFusion not only excels in addressing single-modal

degradation but also effectively tackles more challenging single-modal and multi-modal composite degradation scenarios. In particular, when rain and haze coexist in the visible image, ControlFusion successfully perceives these degradations and eliminates their effects. In multi-modal composite degradation scenarios, it leverages degradation prompts to adjust the distribution of fusion features, achieving high-quality restoration and fusion. Extensive experiments demonstrate that ControlFusion exhibits significant advantages in complex degradation scenarios.

## 5.3. Extended Experiments and Discussions

**Flexible Degree Control.** As shown in Fig. 5, with degradation level prompts, our ControlFusion can adapt to varying degrees of degradation and deliver satisfactory fusion results. Moreover, fusion results generated using adjacent degradation-level prompts exhibit subtle yet perceptible differences, allowing users to obtain customized outcomes through their specific prompts.

**Visual Embedding versus Textual Embedding.** From Fig. 6, we can find that both visual and textual prompts assist  $N_{rf}$  in restoring the scene illumination. Besides, the residual map of both is subtle, indicating that our SFVA successfully captures the degradation type and degree.

**Object Detection.** We further evaluate object detection performance on LLVIP to indirectly assess the fusion quality,

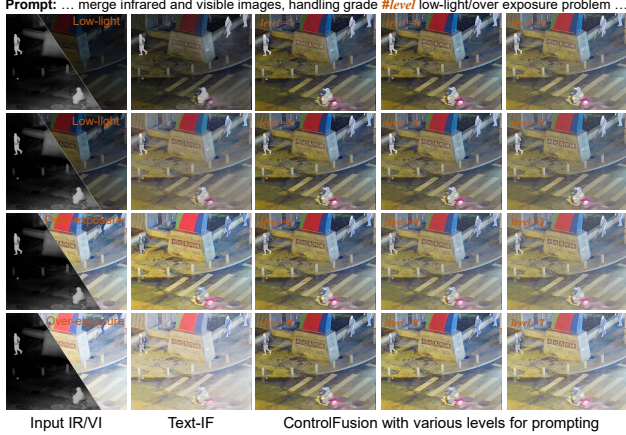


Figure 5. Fusion results with various level prompt.

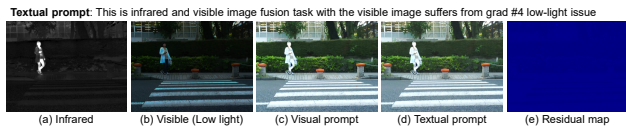


Figure 6. Comparison of visual and textual embedding

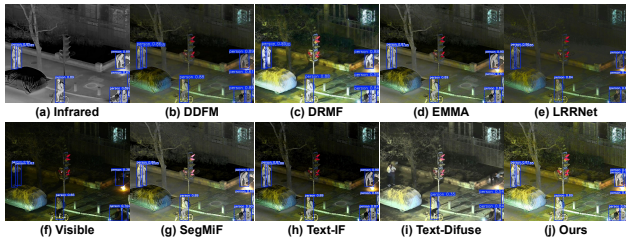


Figure 7. Visual comparison of object detection.

Table 3. Quantitative comparison of object detection.

Methods	Prec.	Recall	AP@0.50	AP@0.75	mAP@0.5:0.95
DDFM [49]	0.947	0.848	0.911	0.655	0.592
DRMF [32]	0.958	0.851	0.937	0.672	0.607
EMMA [50]	0.942	0.872	0.927	0.647	0.598
LRRNet [12]	0.939	0.878	0.933	0.672	0.608
SegMIF [16]	0.965	0.896	0.931	0.690	0.603
Text-IF [38]	0.959	0.892	0.939	0.655	0.601
Text-Difuse [41]	0.961	0.885	0.941	0.656	0.606
ControlFusion	0.971	0.889	0.949	0.685	0.609

using the re-trained YOLOv8 [27]. Qualitative and quantitative results are presented in Fig. 7 and Tab. 3. Due to effective information restoration and integration, our fusion results enable the detector to identify all pedestrians with higher confidence, achieving the highest mAP@0.5-0.95 across various confidence thresholds.

**Real-World Generalization.** As shown in Fig. 8, our method generalizes well to real-world scenarios, benefiting from the proposed physics-driven degraded imaging model. The first scene is captured by our multi-modal sensors with low light and noise degradation, and the second is from the FMB dataset, affected by extreme low light.



Figure 8. Generalization results in the real world.

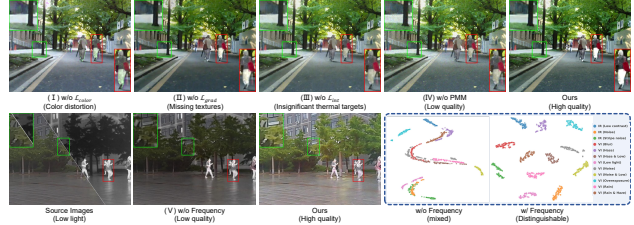


Figure 9. Visualization of ablation experiment results.

Table 4. Quantitative results of the ablation studies.

Configs	VI(LL & Noise)				VI(OE) and IR(LC)				VI(RH) and IR(Noise)			
	CLIP-IQA	MUSIQ	TReS	EN	CLIP-IQA	MUSIQ	TReS	SD	CLIP-IQA	MUSIQ	TReS	SD
I	0.132	42.424	42.839	4.788	0.166	41.983	42.841	39.917	0.147	43.619	47.932	48.935
II	0.152	45.582	45.358	5.855	0.151	43.646	42.002	39.208	0.167	47.862	45.007	44.347
III	0.154	46.571	44.495	5.013	0.155	44.286	44.561	42.068	0.156	43.007	43.816	41.544
IV	0.129	38.960	41.310	5.414	0.172	41.743	39.125	38.748	0.118	48.882	46.245	45.910
V	0.173	45.281	46.291	6.279	0.181	45.386	47.519	46.860	0.149	46.714	48.094	46.950
Ours	0.225	49.333	49.513	7.111	0.187	50.479	50.298	50.955	0.179	50.107	51.091	55.417

**Ablation Studies.** To verify the effectiveness of our key components, we conduct ablation studies across three degradation scenarios. This study involves: (I) **w/o**  $\mathcal{L}_{color}$ , (II) **w/o**  $\mathcal{L}_{grad}$ , (III) **w/o**  $\mathcal{L}_{int}$ , (IV) **w/o** PMM, and (V) **w/o** frequency branch. As shown in Fig. 9, omitting any loss or module significantly impacts the fusion quality. Specifically, without  $\mathcal{L}_{color}$ , color distortion occurs, while removing  $\mathcal{L}_{grad}$  leads to the loss of essential texture information. Excluding  $\mathcal{L}_{int}$  fails to highlight thermal targets, and removing PMM diminishes the ability to address composite degradation. Additionally, removing the frequency branch from SFVA causes visual prompt confusion. The t-SNE results further validate the importance of frequency priors. The quantitative results in Tab. 4 also confirm that each design element is crucial for enhancing fusion performance.

## 6. Conclusion

This work proposes a controllable framework for image restoration and fusion leveraging language-visual prompts. Initially, we develop a physics-driven degraded imaging model to bridge the domain gap between synthetic data and real-world images, providing a solid foundation for addressing composite degradations. Moreover, we devise a prompt-modulated network that adaptively adjusts the fusion feature distribution, enabling robust feature enhancement based on degradation prompts. Prompts can either come from text instructions to support user-defined control or be extracted from source images using a spatial-frequency visual adapter embedded with frequency priors, facilitating automated deployment. Extensive experiments

demonstrate that the proposed method excels in handling real-world and composite degradations, showing strong robustness across various degradation levels.

## References

- [1] Fanglin Bao, Xueji Wang, Shree Hari Sureshbabu, Gautam Sreekumar, Liping Yang, Vaneet Aggarwal, Vishnu N Bodeti, and Zubin Jacob. Heat-assisted detection and ranging. *Nature*, 619(7971):743–748, 2023. 1
- [2] Marcos V Conde, Gregor Geigle, and Radu Timofte. Instructir: High-quality image restoration following human instructions. In *Proceedings of the European Conference on Computer Vision*, 2024. 2, 7
- [3] S Alireza Golestaneh, Saba Dadsetan, and Kris M Kitani. No-reference image quality assessment via transformers, relative ranking, and self-consistency. In *Proceedings of the IEEE Winter Conference on Applications of Computer Vision*, pages 1220–1230, 2022. 6
- [4] Juntao Guan, Rui Lai, and Ai Xiong. Wavelet deep neural network for stripe noise removal. *IEEE Access*, 7:44544–44554, 2019. 7
- [5] Xiaojie Guo, Yu Li, and Haibin Ling. Lime: Low-light image enhancement via illumination map estimation. *IEEE Transactions on Image Processing*, 26(2):982–993, 2016. 3
- [6] Yu Guo, Yuan Gao, Yuxu Lu, Huilin Zhu, Ryan Wen Liu, and Shengfeng He. Onerestore: A universal restoration framework for composite degradation. In *Proceedings of the European Conference on Computer Vision*, pages 255–272. Springer, 2024. 7
- [7] Deepak Kumar Jain, Xudong Zhao, Germán González-Almagro, Chenquan Gan, and Ketan Kotecha. Multimodal pedestrian detection using metaheuristics with deep convolutional neural network in crowded scenes. *Information Fusion*, 95:401–414, 2023. 1
- [8] Xinyu Jia, Chuang Zhu, Minzhen Li, Wenqi Tang, and Wenli Zhou. Lvvip: A visible-infrared paired dataset for low-light vision. In *Proceedings of the IEEE International Conference on Computer Vision*, pages 3496–3504, 2021. 3, 6
- [9] Yitong Jiang, Zhaoyang Zhang, Tianfan Xue, and Jinwei Gu. Autodir: Automatic all-in-one image restoration with latent diffusion. In *Proceedings of the European Conference on Computer Vision*, 2024. 2
- [10] Junjie Ke, Qifei Wang, Yilin Wang, Peyman Milanfar, and Feng Yang. Musiq: Multi-scale image quality transformer. In *Proceedings of the IEEE International Conference on Computer Vision*, pages 5148–5157, 2021. 6
- [11] Hui Li and Xiao-Jun Wu. Densfuse: A fusion approach to infrared and visible images. *IEEE Transactions on Image Processing*, 28(5):2614–2623, 2019. 2
- [12] Hui Li, Tianyang Xu, Xiao-Jun Wu, Jiwen Lu, and Josef Kittler. Lrrnet: A novel representation learning guided fusion network for infrared and visible images. *IEEE Transactions on Pattern Analysis and Machine Intelligence*, 45(9):11040–11052, 2023. 2, 6, 8
- [13] Ruoteng Li, Loong-Fah Cheong, and Robby T Tan. Heavy rain image restoration: Integrating physics model and conditional adversarial learning. In *Proceedings of the IEEE Conference on Computer Vision and Pattern Recognition*, pages 1633–1642, 2019. 3
- [14] Pengwei Liang, Junjun Jiang, Xianming Liu, and Jiayi Ma. Fusion from decomposition: A self-supervised decomposition approach for image fusion. In *Proceedings of the European Conference on Computer Vision*, pages 719–735, 2022. 2
- [15] Jinyuan Liu, Xin Fan, Zhanbo Huang, Guanyao Wu, Risheng Liu, Wei Zhong, and Zhongxuan Luo. Target-aware dual adversarial learning and a multi-scenario multi-modality benchmark to fuse infrared and visible for object detection. In *Proceedings of the IEEE Conference on Computer Vision and Pattern Recognition*, pages 5802–5811, 2022. 2
- [16] Jinyuan Liu, Zhu Liu, Guanyao Wu, Long Ma, Risheng Liu, Wei Zhong, Zhongxuan Luo, and Xin Fan. Multi-interactive feature learning and a full-time multi-modality benchmark for image fusion and segmentation. In *Proceedings of the IEEE International Conference on Computer Vision*, pages 8115–8124, 2023. 2, 3, 6, 8
- [17] Zhu Liu, Jinyuan Liu, Benzhuang Zhang, Long Ma, Xin Fan, and Risheng Liu. Paif: Perception-aware infrared-visible image fusion for attack-tolerant semantic segmentation. In *Proceedings of the ACM International Conference on Multimedia*, pages 3706–3714, 2023. 2
- [18] Ziwei Luo, Fredrik K. Gustafsson, Zheng Zhao, Jens Sjölund, and Thomas B. Schön. Controlling vision-language models for multi-task image restoration. In *International Conference on Learning Representations*, 2024. 3, 7
- [19] Jiayi Ma, Wei Yu, Pengwei Liang, Chang Li, and Junjun Jiang. Fusiongan: A generative adversarial network for infrared and visible image fusion. *Information Fusion*, 48:11–26, 2019. 2
- [20] Jiayi Ma, Linfeng Tang, Meilong Xu, Hao Zhang, and Guobao Xiao. Stdfusionnet: An infrared and visible image fusion network based on salient target detection. *IEEE Transactions on Instrumentation and Measurement*, 70:5009513, 2021. 2
- [21] Jiayi Ma, Linfeng Tang, Fan Fan, Jun Huang, Xiaoguang Mei, and Yong Ma. Swinfusion: Cross-domain long-range learning for general image fusion via swin transformer. *IEEE/CAA Journal of Automatica Sinica*, 9(7):1200–1217, 2022. 2, 5
- [22] Earl J McCartney. Optics of the atmosphere: scattering by molecules and particles. *New York*, 1976. 3
- [23] Amanda C Muller and Sundaram Narayanan. Cognitively-engineered multisensor image fusion for military applications. *Information Fusion*, 10(2):137–149, 2009. 1
- [24] Vaishnav Potlapalli, Syed Waqas Zamir, Salman H Khan, and Fahad Shahbaz Khan. Promptir: Prompting for all-in-one image restoration. *Advances in Neural Information Processing Systems*, 36, 2024. 2
- [25] Chenyang Qi, Zhengzhong Tu, Keren Ye, Mauricio Delbracio, Peyman Milanfar, Qifeng Chen, and Hossein Talebi. Spire: Semantic prompt-driven image restoration. In *Proceedings of the European Conference on Computer Vision*, pages 446–464. Springer, 2024. 2

- [26] Alec Radford, Jong Wook Kim, Chris Hallacy, Aditya Ramesh, Gabriel Goh, Sandhini Agarwal, Girish Sastry, Amanda Askell, Pamela Mishkin, Jack Clark, et al. Learning transferable visual models from natural language supervision. In *Proceedings of the International Conference on Machine Learning*, pages 8748–8763, 2021. 2, 4
- [27] Joseph Redmon, Santosh Divvala, Ross Girshick, and Ali Farhadi. You only look once: Unified, real-time object detection. In *Proceedings of the IEEE Conference on Computer Vision and Pattern Recognition*, pages 779–788, 2016. 8
- [28] Linfeng Tang, Yuxin Deng, Yong Ma, Jun Huang, and Jiayi Ma. Superfusion: A versatile image registration and fusion network with semantic awareness. *IEEE/CAA Journal of Automatica Sinica*, 9(12):2121–2137, 2022. 2
- [29] Linfeng Tang, Jiteng Yuan, and Jiayi Ma. Image fusion in the loop of high-level vision tasks: A semantic-aware real-time infrared and visible image fusion network. *Information Fusion*, 82:28–42, 2022. 2
- [30] Linfeng Tang, Jiteng Yuan, Hao Zhang, Xingyu Jiang, and Jiayi Ma. Piafusion: A progressive infrared and visible image fusion network based on illumination aware. *Information Fusion*, 83:79–92, 2022. 2, 3, 6
- [31] Linfeng Tang, Xinyu Xiang, Hao Zhang, Meiqi Gong, and Jiayi Ma. Divfusion: Darkness-free infrared and visible image fusion. *Information Fusion*, 91:477–493, 2023. 2
- [32] Linfeng Tang, Yuxin Deng, Xunpeng Yi, Qinglong Yan, Yixuan Yuan, and Jiayi Ma. Drmf: Degradation-robust multi-modal image fusion via composable diffusion prior. In *Proceedings of the ACM International Conference on Multimedia*, pages 8546–8555, 2024. 2, 6, 8
- [33] Di Wang, Jinyuan Liu, Xin Fan, and Risheng Liu. Unsupervised misaligned infrared and visible image fusion via cross-modality image generation and registration. In *Proceedings of the International Joint Conference on Artificial Intelligence*, pages 3508–3515, 2022. 2
- [34] Jianyi Wang, Kelvin CK Chan, and Chen Change Loy. Exploring clip for assessing the look and feel of images. In *Proceedings of the AAAI Conference on Artificial Intelligence*, pages 2555–2563, 2023. 6
- [35] Han Xu, Jiayi Ma, Zhuliang Le, Junjun Jiang, and Xiaojie Guo. Fusiondn: A unified densely connected network for image fusion. In *Proceedings of the AAAI Conference on Artificial Intelligence*, 2020. 6
- [36] Han Xu, Jiayi Ma, Junjun Jiang, Xiaojie Guo, and Haibin Ling. U2fusion: A unified unsupervised image fusion network. *IEEE Transactions on Pattern Analysis and Machine Intelligence*, 44(1):502–518, 2022. 3
- [37] Han Xu, Jiteng Yuan, and Jiayi Ma. Murf: Mutually reinforcing multi-modal image registration and fusion. *IEEE Transactions on Pattern Analysis and Machine Intelligence*, 45(10):12148–12166, 2023. 2
- [38] Xunpeng Yi, Han Xu, Hao Zhang, Linfeng Tang, and Jiayi Ma. Text-if: Leveraging semantic text guidance for degradation-aware and interactive image fusion. In *Proceedings of the IEEE Conference on Computer Vision and Pattern Recognition*, pages 27026–27035, 2024. 2, 5, 6, 8
- [39] Syed Waqas Zamir, Aditya Arora, Salman Khan, Munawar Hayat, Fahad Shahbaz Khan, and Ming-Hsuan Yang. Restormer: Efficient transformer for high-resolution image restoration. In *Proceedings of the IEEE Conference on Computer Vision and Pattern Recognition*, pages 5728–5739, 2022. 3
- [40] Hao Zhang, Han Xu, Xin Tian, Junjun Jiang, and Jiayi Ma. Image fusion meets deep learning: A survey and perspective. *Information Fusion*, 76:323–336, 2021. 1
- [41] Hao Zhang, Lei Cao, and Jiayi Ma. Text-difuse: An interactive multi-modal image fusion framework based on text-modulated diffusion model. *Advances in Neural Information Processing Systems*, 37:39552–39572, 2025. 2, 6, 8
- [42] Jing Zhang, Aiping Liu, Dan Wang, Yu Liu, Z Jane Wang, and Xun Chen. Transformer-based end-to-end anatomical and functional image fusion. *IEEE Transactions on Instrumentation and Measurement*, 71:5019711, 2022. 2
- [43] Jiaming Zhang, Huayao Liu, Kailun Yang, Xinxin Hu, Ruiping Liu, and Rainer Stiefelhagen. Cmx: Cross-modal fusion for rgb-x semantic segmentation with transformers. *IEEE Transactions on Intelligent Transportation Systems*, 24(12):14679–14694, 2023. 1
- [44] Xingchen Zhang and Yiannis Demiris. Visible and infrared image fusion using deep learning. *IEEE Transactions on Pattern Analysis and Machine Intelligence*, 45(8):10535–10554, 2023. 1
- [45] Yue Zhang, Bin Song, Xiaojiang Du, and Mohsen Guizani. Vehicle tracking using surveillance with multimodal data fusion. *IEEE Transactions on Intelligent Transportation Systems*, 19(7):2353–2361, 2018. 1
- [46] Hang Zhao, Orazio Gallo, Iuri Frosio, and Jan Kautz. Loss functions for image restoration with neural networks. *IEEE Transactions on Computational Imaging*, 3(1):47–57, 2016. 5
- [47] Wenda Zhao, Shigeng Xie, Fan Zhao, You He, and Huchuan Lu. Metafusion: Infrared and visible image fusion via meta-feature embedding from object detection. In *Proceedings of the IEEE Conference on Computer Vision and Pattern Recognition*, pages 13955–13965, 2023. 2
- [48] Zixiang Zhao, Haowen Bai, Jianshe Zhang, Yulun Zhang, Shuang Xu, Zudi Lin, Radu Timofte, and Luc Van Gool. Cddfuse: Correlation-driven dual-branch feature decomposition for multi-modality image fusion. In *Proceedings of the IEEE Conference on Computer Vision and Pattern Recognition*, pages 5906–5916, 2023. 2
- [49] Zixiang Zhao, Haowen Bai, Yuanzhi Zhu, Jianshe Zhang, Shuang Xu, Yulun Zhang, Kai Zhang, Deyu Meng, Radu Timofte, and Luc Van Gool. Ddfm: Denoising diffusion model for multi-modality image fusion. In *Proceedings of the IEEE International Conference on Computer Vision*, pages 8082–8093, 2023. 2, 6, 8
- [50] Zixiang Zhao, Haowen Bai, Jianshe Zhang, Yulun Zhang, Kai Zhang, Shuang Xu, Dongdong Chen, Radu Timofte, and Luc Van Gool. Equivariant multi-modality image fusion. In *Proceedings of the IEEE Conference on Computer Vision and Pattern Recognition*, pages 25912–25921, 2024. 2, 6, 8

# ControlFusion: A Controllable Image Fusion Framework with Language-Vision Degradation Prompts

## Supplementary Material

Table 5. Hyper-parameters of different degradation types

Degradations	$\alpha_{int}$	$\alpha_{ssim}$	$\alpha_{grad}$	$\alpha_{color}$
Blur	3	1	15	12
Rain	5	1	14	12
Haze	4	1	8	12
Low-light	8	1	10	12
Low-contrast	8	1	10	12
Stripe noise	6	0	12	12
Over-exposure	4	0	2	7
Noise (IR & VI)	6	1	10	12
Rain & Haze	5	1	12	12
Haze & Low-light	7	1	11	12
Noise & Low-light	7	1	10	12

Table 6. Details of network architecture

	Num blocks	Attention heads	FFN factor	Basic dim
Values	[2,2,2,2]	[1,2,4,8]	2	48

### A. Hyper-parameters across Various Degradations

To enable the unified restoration and fusion network to adapt to various degradation types, we not only need to use degradation cues to modulate the fusion features but also customize hyper-parameters for each set of degradation types. This ensures that the model is optimized along the optimal path. Particularly, in addressing diverse degradation scenarios encountered across different data modalities, we systematically explore and iteratively refine hyper-parameter combinations through extensive empirical experimentation, ultimately identify parameter sets that demonstrate robust performance improvements. The finalized hyper-parameter selections, representing the most effective configurations derived from this comprehensive optimization process, are explicitly tabulated in Tab. 5.

### B. Details of Network Architecture

This framework uses a symmetric encoder structure to process multi-modal inputs separately. Each encoder contains a multi-stage feature extraction module, and progressive feature extraction is achieved through cascaded Transformer blocks. The decoder uses a multi-level up-sampling architecture to achieve resolution recovery, and each level fuses the feature maps of the corresponding encoding stage. We employ the ViT-L/14@336px of CLIP as the text encoder to ensure semantic consistency. The specific parameter config-

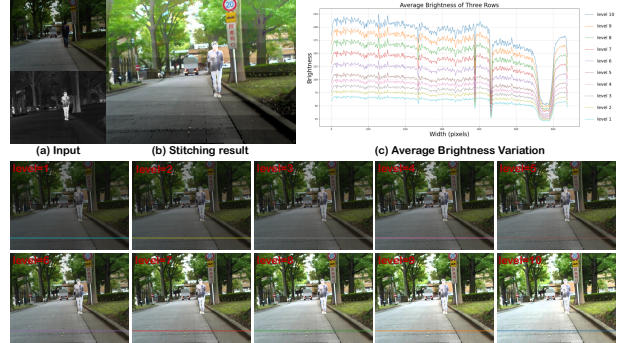


Figure 10. Visualization of continuous degradation level control.

Table 7. Comparison of model parameters, computational complexity and average testing time of different methods

Methods	Fusion			Fusion with enhancement		
	parm.(m)	flops(g)	time(s)	parm.(m)	flops(g)	time(s)
DDFM	552.700	5220.000	34.500	779.590	6018.200	34.910
DRMF	5.050	121.100	0.842	170.900	4575.800	1.979
EMMA	1.516	41.540	<b>0.037</b>	228.450	839.230	0.440
LRRNet	<b>0.049</b>	<b>14.170</b>	0.085	226.980	<b>811.860</b>	0.488
SegMiF	45.040	353.700	0.147	271.970	1151.400	0.550
Text-Difuse	157.350	4872.000	31.630	157.350	4872.000	31.630
Text-IF	89.010	1518.900	0.157	<b>89.010</b>	1518.900	<b>0.157</b>
ControlFusion	123.898	327.980	0.344	123.898	<b>327.980</b>	0.344

uration of the model is shown in Tab. 6.

### C. Computational efficiency comparison

We assess the computational efficiency of ControlFusion in comparison with SOTA methods. In scenarios where the enhancement algorithm is excluded, our method does not exhibit significant competitiveness. Nevertheless, when addressing the enhancement-fusion task, our approach demonstrates superior performance. Quantitative comparisons are presented in Tab. 7.

### D. Visualization of continuous degradation level control

Although we use four discrete degradation levels to train our prompt-modulated restoration and fusion network, thanks to the powerful text parsing ability of CLIP, our model is able to achieve continuous degree control. As shown in Fig. 10, under low-light conditions, as we increase the degradation level from 1 to 10, the exposure level of the fusion results also increases. In addition, as illustrated in Fig. 10 (c), the average brightness of the three rows also increases with the degradation level prompts.